Structural properties of liquid Al$_2$O$_3$: A molecular dynamics study

Gonzalo Gutiérrez, A. B. Belonoshko, Rajeev Ahuja, and Börje Johansson
Condensed Matter Theory Group, Department of Physics, Uppsala University, Box 530, S-751 21 Uppsala, Sweden

Molecular dynamics (MD) simulations of liquid aluminum oxide (Al$_2$O$_3$) were carried out on a system with up to 1800 particles, using a pairwise potential. All simulations were done in the microcanonical ensemble, for two densities, 3.0 and 3.175 g/cm^3, at temperatures of 2200, 2600, and 3000 K. A detailed analysis of the interatomic distances, given by the partial pair-distribution functions and the bond-angles distribution, reveals that in the liquid state there is a short range order dominated by a somewhat distorted $(AlO_4)^{5-}$ tetrahedron, in agreement with recent experimental measurements. This conclusion is supported by the distribution of nearest-neighbor coordinations, where more than 60% of Al atoms have four O as nearest neighbors. This finding does not change over the explored temperature range. Because of the presence of twofold rings, the connectivity of $(AlO_4)^{5-}$ units consists of corner, edge, and face sharing tetrahedra. Based in this structural information, i.e., bond lengths, coordination numbers, bond-angle distributions, and ring statistics, our MD simulation allows us to put forward a possible structure of liquid Al$_2$O$_3$.

PACS number(s): 61.20.Ja, 61.25.$-$f

I. INTRODUCTION

Aluminum oxide, Al$_2$O$_3$, traditionally referred to as alumina, is a very important ceramic material with many technological applications. Its great usefulness as a technological system rests primarily on its extreme hardness (Moh 9), high melting point (2327 K), and low electrical conductivity (10^{-12} S/m at 20 °C). It has a wide range of applications, from electronics, optics, biomedical and mechanical engineering to catalyst support. Crystal polymorphs of alumina, particularly its thermodynamically stable phase α-Al$_2$O$_3$, or corundum, have been studied rather extensively, both experimentally and theoretically, with emphasis on properties and phase transitions at room temperature. In spite of that, there are many metastable structures which so far are not well understood (see for example, Ref. [1], and for a more recent review see Ref. [2]).

Liquid alumina is also of great interest both from the experimental and theoretical points of view. It is a well-recognized reference material in high temperature applications, hence knowledge of its properties is essential for industrial application in materials processing such as sintering reaction for producing new ceramics [3]. In addition, molten alumina is one of the precursors for the allotropic form γ-Al$_2$O$_3$, and atomic-level information about its structure would be very useful to understand the transition towards the stable α-Al$_2$O$_3$ phase.

However, in contrast to the crystal phases, only a few studies exist about liquid alumina. This is partially due to the difficulties of doing experimental studies at elevated temperatures, and also because the theoretical approaches employed are usually restricted to applications at 0 K. For liquid alumina, there are measurements of its volume expansion [4] and optical properties [5,6]. Recently, the Al coordination numbers have been estimated from NMR measurements in liquid Al$_2$O$_3$ [7,8] and in glass as well as in liquid Al$_2$O$_3$-SiO$_2$ [9,10]. Also, solidification behavior [11] and the pressure dependence of its melting temperature [12] have been reported.

As far as the structural properties of liquid alumina are concerned, two experimental studies have been published recently, one by Waseda *et al.* [13] and the other by Ansell *et al.* [14]. Unfortunately their results are in disagreement with each other. The measurements of Waseda and *et al.* were done by means of x-ray diffraction technique, at the temperature of 2363 K. The radial distribution function was estimated by using the interference function refining technique, assuming a density $\rho = 3.01$ g/cm^3, obtaining for the pair distribution function a first peak at 2.0 Å and a second peak at 2.8 Å. They have also calculated the partial distribution functions, obtaining for nearest neighbor interatomic distances Al—O, O—O, and Al—Al, the values 2.02 Å, 2.82 Å, and 2.87 Å, respectively. The Al coordination number was estimated to be 5.6. Thus, octahedrally coordinated aluminum is found as the fundamental cluster configuration in the melt. These results contradict the ones found by Ansell *et al.*, who reported measurements using x-ray synchrotron radiation at 2663 K and 2223 K. They used the maximum entropy Fourier transform method, assuming a density of 3.175 g/cm^3, to obtain the pair distribution function. The first peak is at 1.76 Å and the second peak at 3.08 Å, and the Al coordination number was estimated in 4.4 ± 1.0. These results imply that Al$_2$O$_3$ undergoes a major structural rearrangement on melting, with an Al coordination change from octahedral (solid phase) to tetrahedral (liquid phase), which remains over a temperature range of 500 K. The interatomic distances were estimated to be 1.76 Å for Al—O and 3.08 Å for O—O. No explanation that might account for this discrepancy with the results of Waseda *et al.* has been provided by Ansell *et al.* It should be noted that in the former experiment the sample was heated in a molybdenum cell, whereas in the second one the specimens were levitated in a conical nozzle and melted with a laser. However, the coordination number found by Ansell *et al.* is supported by the measurements done by Coutures *et al.* [7] and Massiot *et al.* [8] using ^{27}Al magic-angle spining NMR spectroscopy on liquid Al$_2$O$_3$, from which it is inferred that liquid consists of predominantly four-coordinated Al^{3+}, with

an average Al coordination number of 4.5 ± 1.0. Similar NMR results have been obtained for the Al_2O_3-SiO_2 system, both for glass quenched from the melt [9] as well as for liquid [10]. Moreover, quenched experiments do support this proposed tetrahedral coordination above the melting point because high cooling rates ($>10^5$ K/s) from melt result in crystallization of either γ-Al_2O_3 or various ordered transition Al_2O_3 phases, all containing tetrahedrally coordinated aluminum [15].

In view of the above discrepancies, it would be very interesting to perform a theoretical study on the structure of liquid Al_2O_3 which might contribute to resolving this controversy. Molecular dynamics (MD) techniques [16] seem well suited to tackle the type of problems at hand. In fact, three recent MD works have obtained interesting results using pair potentials. In Refs. [17,18], the authors calculated the melting temperature with respect to the pressure using the so-called ''two-phase methods,'' obtaining a close agreement with the experimental values. They also presented the pair distribution function at 2663 K. San Miguel *et al.* [19] have performed MD simulations for systems at temperatures ranging from 2200 K to 3000 K. They have found that the liquid structure is invariant as a function of temperature at constant volume, and concluded that more than 50% of Al atoms are tetrahedrally coordinated at four different temperatures. These three papers are in good agreement with the results of Ansell *et al.*, giving support to the thesis that short range order in molten alumina is defined essentially by a $(AlO_4)^{5-}$ basic unit.

In this contribution we report on a MD study of liquid Al_2O_3. Our main goal is to investigate in detail the short and intermediate range order of the liquid structure as inferred from the pair-distribution function, coordination number, and bond-angle distribution. We will also discuss the effect of temperature and pressure on these properties. The present paper is organized as follows: after this introduction, in Sec. II we present an outline of the MD simulations for liquid Al_2O_3. Results for pair-distribution functions, bond-angle distributions, and rings statistics are presented in Sec. III. A discussion of our findings and the conclusion are drawn in Sec. IV

II. COMPUTATIONAL PROCEDURE

Molecular dynamics simulations are carried out in the microcanonical ensemble (*NVE*) for $N = 1800$ atoms (720 Al and 1080 O), in an orthorhombic cell, using periodic boundary conditions. Two systems were prepared, at mass densities of $\rho_a = 3.0$ g/cm^3 and $\rho_b = 3.175$ g/cm^3, in order to compare with reported experiments [13,14], and run at three different temperatures, $T = 2200$ K, $T = 2600$ K, and $T = 3000$ K. The cell box lengths are $L_x = 27.175$ Å, $L_y = 26.148$ Å, and $L_z = 28.580$ Å for the low density system and $L_x = 26.667$ Å, $L_y = 25.659$ Å, and $L_z = 28.045$ Å for the high density system.

A major issue in MD is the choice of the interaction potential. In addition to some *ab initio* MD simulations on alumina [20,21], a number of interatomic potentials have been developed to study Al_2O_3 in its different phases [22–28]. Following previous works [17,18], we have adopted the transferable potential of Matsui [25], which is still simple

TABLE I. Potential parameters for Al_2O_3.

	$q(|e|)$	A (Å)	B (Å)	C (Å^3 kJ$^{1/2}$ mol$^{-1/2}$)
Al	1.4175	0.7852	0.034	36.82
O	-0.9450	1.8215	0.138	90.61

and has been demonstrated to reproduce a number of experimental properties such as structure, density, bulk modulus, thermal expansivities, and melting temperatures among others [29,30]. The potential employs pairwise additive interatomic terms of the forms

$$V(r_{ij}) = \frac{q_i q_j}{r_{ij}} - \frac{C_i C_j}{r_{ij}^6} + D(B_i + B_j)\exp\left(\frac{A_i + A_j - r_{ij}}{B_i + B_j}\right) \tag{2.1}$$

where the terms represent Coulomb, van der Waals, and repulsion energy, respectively. Here r_{ij} is the interatomic distance between atoms i and j, and D is a standard force constant 4.184 kJ Å^{-1} mol^{-1}. The effective charge q, the repulsive radius A, the softness parameter B, and the van der Waals coefficients C are the energy parameters, which are listed in Table I. The long range Coulomb interactions are calculated with the Ewald summation technique. In the simulation, the equations of motion are integrated with a modification of the Beeman algorithm [31], using a time step $\Delta t = 1 \times 10^{-15}$ s. All the calculations were done using the MOLDY program [31].

The Al_2O_3 liquid systems were generated by starting with an initial orthorhombic lattice corresponding to α-Al_2O_3 at the density of 2.75 g/cm^3. This initial low density system was chosen in order to have a liquid at 5000 K at zero pressure [18], and also to avoid the unphysically attractive features of the potential at very short distance, as is discussed in Ref. [32] for this kind of potential. Thus, this initial configuration is heated to 5000 K and thermalized for over 45 000 time steps. Then, the sample is cooled to 3000 K and thermalized for over 55 000 Δt. In the thermalization process the temperature was lowered with velocity scaling at intervals of 10 time steps during the first 10 000 Δt, after that the system is allowed to reach the equilibrium without any disturbance. With this well-equilibrated Al_2O_3 liquid at 3000 K we prepare the two systems, reducing simultaneously the lengths of the MD cell and the position of all the atoms. From this stage we thermalized the systems at 3000 K for over 45 000 Δt. Preliminary simulations were tried with different schedules and different initial configurations, but no significant differences were found.

III. RESULTS

Complete information on the structural correlations of the simulated liquid can be inferred from pair-distribution functions, coordination numbers, bond-angle distributions, and ring statistics. Atomic trajectories from MD simulations are used to calculate these kinds of positional and angular correlations. All structural properties are calculated by taking the average over the last 100 configurations, separated by 100 time steps. In the case of the pair-distribution function,
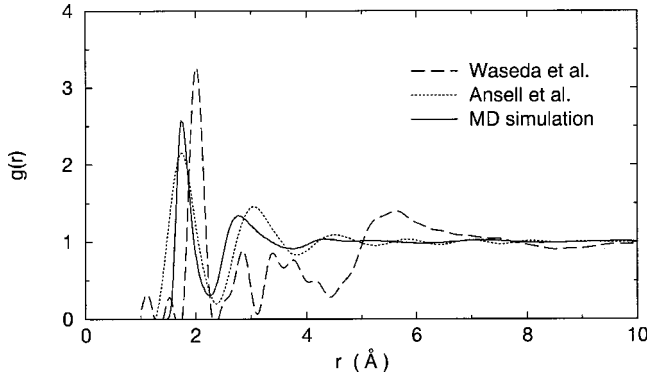
FIG. 1. Total pair-distribution function for liquid Al$_2$O$_3$. Dashed and dotted line, experimental results of Waseda *et al.* and Ansell et al., respectively. Solid line, MD result.

we take an average over 2000 configurations separated by 10 time steps.

A. Pair-distribution function

Basic information about structural correlations is derived from the partial pair-distribution functions $g_{\alpha\beta}$. In a binary system these are determined from

$$g_{\alpha,\beta}(r) = \frac{\langle n_{\alpha,\beta}(r, r + \Delta r) \rangle}{4\pi r^2 \Delta r} \frac{V}{N_\beta}, \quad (\alpha, \beta = \text{Al}, \text{O}), \quad (3.1)$$

where $\langle n_{\alpha,\beta}(r, r + \Delta r) \rangle$ denotes the average number of particles of species β surrounding a particle of species α in a spherical shell between r and $r + \Delta r$, and N_β is the total number of particles of species β (being $N = N_\alpha + N_\beta$ the total number of particles in the system). The total pair-distribution functions are obtained from

$$g(r) = \sum_\alpha \sum_\beta c_\alpha c_\beta g_{\alpha\beta}(r), \quad (3.2)$$

where $c_{\alpha(\beta)} = N_{\alpha(\beta)}/N$ is the concentration of $\alpha(\beta)$ species.

The total pair-distribution functions $g(r)$ from the work of Waseda *et al.* and from the work of Ansell *et al.* are shown in Fig. 1. Together with these experimental estimates, we plot our computed $g(r)$ corresponding to the system at density 3.175 g/cm^3 and temperature of 2200 K. The two experimental results are quite different from one another, as we already pointed out. The computed $g(r)$ shows a better agreement with the results of Ansell *et al.*, especially in the first peak, although at distances beyond 5 Å the curves differ. In spite of that, the simulated liquid reproduces the experimental results of Ansell *et al.* at short distances very well, as we will show below.

In Figs. 2(a) and 2(b) we show the computed total pair-distribution functions at two different densities and at three temperatures. From Fig. 2(a), which corresponds to the lower density system, we can see that the only change which happened under pressure is related with the height of the peaks, whereas the position remains almost the same. Similar behavior is shown in Fig. 2(b) corresponding to the high density system. Comparing Figs. 2(a) and 2(b), we notice that while the first peak is located at the same position in both figures, 1.75 Å, the second peak shifts to the left, from
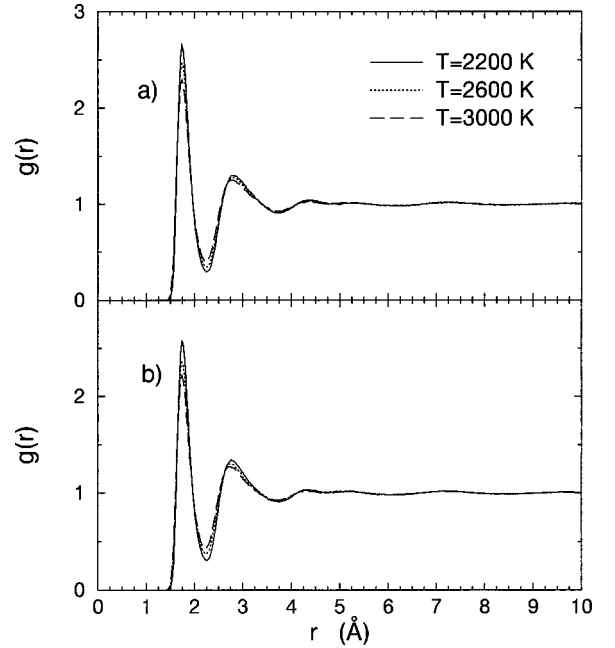

FIG. 2. Total pair-distribution function for liquid Al$_2$O$_3$, calculated at three different temperatures, $T = 2200$, $T = 2600$, and $T = 3000$ K, and at two different densities, (a) $\rho_a = 3.0$ g/cm^3 and (b) $\rho_b = 3.175$ g/cm^3.

2.85 Å in the low density system to 2.80 Å in the high density system. The other features of the curves are almost the same. In both systems the Al coordination number is 4.4, calculated with a cutoff located at the first minima of $g(r)$. Thus, regarding the density of liquid alumina, aside from the shift in the second peak, no significant changes were found in the range explored which roughly corresponds to the experimental density value [33,38]. With respect to the behavior at different temperatures, the only noticeable changes are the heights and widths of the peaks: the higher the temperature, the lower and wider is the peak. This is an expression of the increased disorder with temperature. The same trend is found in the partial pair-distribution function as well as in the angle distribution. These results agree well with the ones of Ansell *et al.*, except for the position of the second peak, for which the value obtained in our simulation is smaller, as in the case of the work of San Miguel *et al.*, and for the width of the peaks they are narrower than the experimental ones. Based on these considerations, we will in the rest of this paper extract conclusions for the results of the high density system, $\rho_b = 3.175$ g/cm^3, at $T = 2200$ K, which corresponds to the supercooled system of Ansell *et al.*

The partial pair-distribution functions are shown in Fig. 3. We find that the Al—O and O—O bond lengths, given by the positions of the first peak in $g_{\text{Al-O}}$ and $g_{\text{O-O}}$, are 1.75 Å and 2.75 Å, and the corresponding full width at half maximum (FWHM) are 0.4 Å and 0.6 Å, respectively. The nearest-neighbor distance for Al—Al is 3.15 ± 0.4 Å. It is clear from this figure that the second peak of $g(r)$ is due to a superposition of O—O and Al—Al nearest-neighbor distances, and not only due to O—O closest distance. Also, the third peak of the total pair-distribution function at 4.25 Å, according to this simulation, comes from the Al—O second nearest neighbors, and not from O—O next nearest neigh-
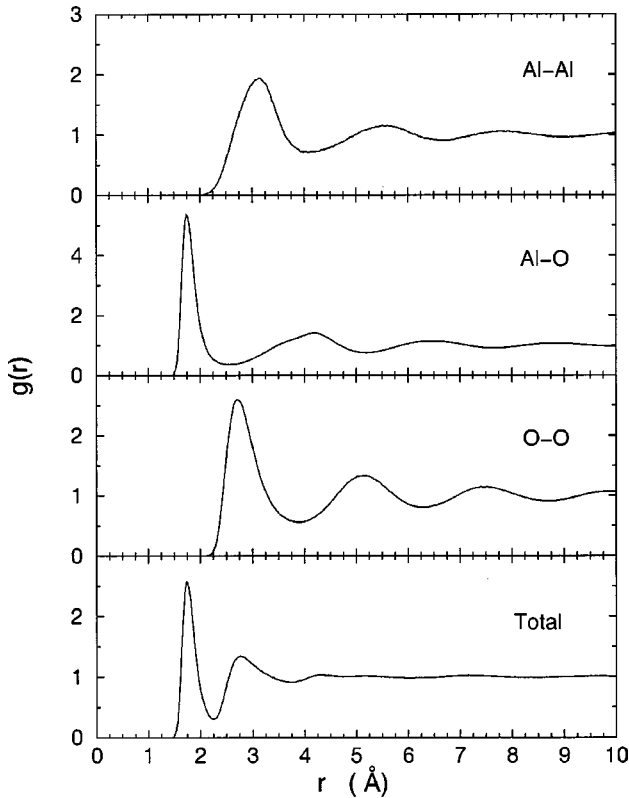
FIG. 3. Partial pair-distribution function for liquid Al_2O_3, att he density $\rho_b = 3.175$ g/cm^3 and temperature $T = 2200$ K.

bors (at 5.15 Å), as was suggested by Ansell *et al.*

In order to obtain more information about the short range correlations, it is essential to supplement the information of the bond lengths with the nearest-neighbors coordination numbers. The average coordination number $n_{\alpha\beta}$ is calculated from

$$n_{\alpha\beta}(R) = 4\pi c_\beta n \int_0^R g_{\alpha\beta}(r) r^2 dr, \qquad (3.3)$$

where $n = N/V$ is the average number density. Thus, within the cutoff distance $R_{Al-O} = 2.2$, $R_{O-O} = 3.2$ and $R_{Al-Al} = 3.7$ Å, the Al atom is on the average surrounded by 8.24 Al atoms and 4.1 O atoms, while the O atom is surrounded by 2.72 Al atoms and 8.84 O atoms. Figure 4 shows histograms with the distribution of coordination numbers for different kinds of neighbors at three different temperatures. We can see that at $T = 2200$ K, more than 60% of the Al atoms have tetrahedral coordination, and more than 60% of the O atoms have three Al atoms as first nearest neighbors. The coordination number for Al—Al is peaked at 8 and for O—O it is peaked at 9. Note that the number of Al atoms coordinated with six oxygen atoms is small, suggesting that the presence of AlO_6 octahedra, if present at all, must be very small (less than 2%).

Although these numbers change very little over the range of temperatures considered, we can see that in the Al—O coordination number, the fraction of three-coordinated Al atoms inscreases with temperature, whereas the fraction of four- and five-coordinated Al decreases. In the case of O—Al coordination number, the fraction of two- and four-
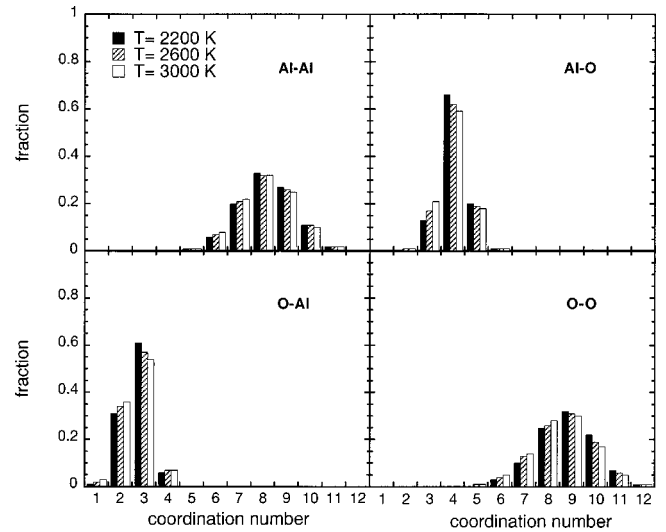

FIG. 4. Distribution of Al and O nearest-neighbors coordination in liquid Al_2O_3, at the density $\rho_b = 3.175$ g/cm^3, at three different temperatures: 2200 K, 2600 K, and 3000 K.

coordinated O atoms increases a little at the expense of the three-coordinated O atoms. The overall picture can be seen as a consequence of increased disorder and interdiffusion when the temperature increases. In fact, this trend remains the same when one decreases the temperature and obtains an amorphous system, where the distribution of coordination number presents a clear maxima at four-coordinated Al and three-coordinated O [34].

B. Angle distributions

Valuable information about the local structural units and their connectivity in the liquid is provided by the bond-angle distribution $P_{\alpha\beta\gamma}(\theta)$. Figure 5 displays the bond-angle distribution calculated with Al—O, O—O, and Al—Al cutoff distances of 2.2, 3.2, and 3.7 Å, respectively. The O—Al—O bond angle distribution has a peak at 95°, Al—O—O at 40° and O—O—O at 60°, with FWHM of 30°, 10°, and 10°, respectively. Knowing that the coordination number of Al is around four, and combining these results with the interatomic distance, we can conclude that the basic unit in molten alumina is a somewhat distorted tetrahedron $(AlO_4)^{-5}$, where the oxygen atoms at the vertices forms a nearly perfect tetrahedron, but where the Al atom is not placed at the very center. The bond angles in an ideal tetrahedron are $\angle$O—Al—O$= 109.47°$, $\angle$O—O—O$= 60°$ and $\angle$Al—O—O$= 35.26°$.

The connectivity of these tetrahedra can be ascertained through the remaining bond-angles and rings analysis. In Fig. 5 the distribution of Al—Al—Al displays a peak around 60°, and a hump between 80 to 120°. The distribution of Al—O—Al angles, which tells us about the connectivity of two basic units, shows a peak at 115°, with a FWHM of 50°. So, Al atoms are linked to O atoms at 115°, and at the same time, Al atoms form an equilateral angle. Taking into account that the coordination number of O—Al is peaked at 3, we can assert that there is one O atom nearly at the center of this triangle. This picture is supported by the Al—Al—O distribution angle, which has one small peak at 35°.
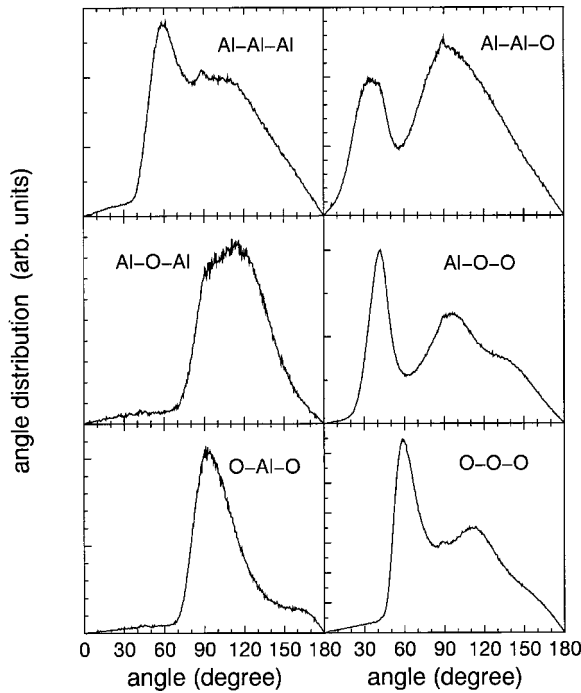
FIG. 5. Bond-angle distribution for liquid Al$_2$O$_3$ at the density $\rho_b = 3.175$ g/cm^3 and the temperature $T = 2200$ K.
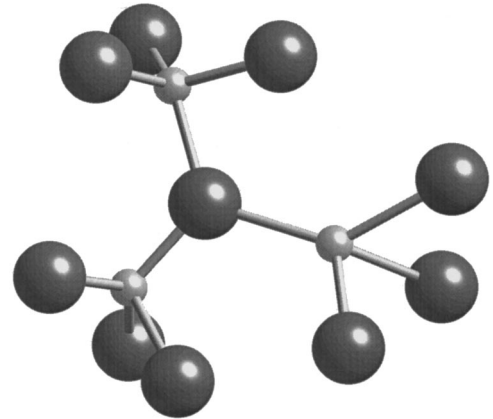

FIG. 6. A typical representative polyhedron found in the simulation. The small spheres correspond to aluminum atoms and the big spheres to oxygen atoms.

To gain insight into network topology, we have calculated the rings statistics. An n-fold ring is defined as the shortest path of alternating Al—O bonds. Thus, starting with an Al atom we locate the positions of the rest of the atoms around it, within a sphere with a cutoff radius of 2.2 Å. Then, the nearest-neighbors O atoms of the central Al are determined. Moving to one of the O atoms, we determine its nearest-neighbors Al atoms, excluding the previous Al atom. This procedure is continued until one of the atoms in the $(n+1)$th sequence corresponds to the central atom. Therefore, n-fold rings consist of $2n$ alternating Al—O bonds. For example, corundum has 40% of twofold and 60% of threefold rings whereas θ-alumina has 23% of twofold rings, 62% of threefold rings, and 15% of fourfold rings. In liquid alumina we found a nearly symmetric distribution, from two- to sevenfold rings, with a peak at fourfold rings (31.6%), followed by threefold rings (24.6%), fivefold rings (22.6%), and a few six- (7.5%) and sevenfold rings (1.1%). Because of the presence of twofold rings (13%), the connectivity of $(AlO_4)^{-5}$ units consists not only of corner, but also of edge and face sharing tetrahedra.

C. Structural model of liquid Al$_2$O$_3$

From the calculated information, we now put forward a structural model of liquid alumina. Figure 6 displays a snapshot of typical structural units and their connectivity found in the simulation. According to our results, this polyhedron corresponds to the majority building blocks in the system. In fact, as was show in Fig. 4, more than 60% Al atoms belong to a $(AlO_4)^{-5}$ tetrahedron. Moreover, this picture is consistent with the rest of the coordination numbers: each Al is coordinated with four O, and in its turn, each O is coordinated with two others Al atoms, giving an Al—Al coordination number of 8. In the same way, we can see from Fig. 6

that each O is coordinated with nine oxygen, in correspondence with the peaks show in Fig. 4.

Of course, there are other possible connections of the tetrahedra. There are approximately 35% of O atoms with coordination 2, which means that the link is only between two tetrahedra, and it can be corner, edge, or face sharing tetrahedra. Also, we can still have an O atom linking four tetrahedra, although its number must be very small (less than 8%).

Finally, we also note that tetrahedron as a basic unit is not the only possibility. Roughly 40% of the Al atoms have both coordination 3 and 5, so we must also expect other kinds of structures compatible with the same interatomic distances and bond angles.

IV. DISCUSSION AND CONCLUSION

A MD calculation based on the two body potential in Eq. (2.1) was implemented to model liquid alumina. The results provide considerable insight into the atomic-level structure of the system, and appear similar to those obtained by San Miguel et al. using a different interatomic potential and a different preparation of the system. Both simulations are in good agreement with the experimental results reported by Ansell et al., except for the position of the second peak in the total pair-distribution function. The experimental value, 3.01 Å, is greater than the value found in the MD simulations: 2.9 Å in the work of San Miguel et al. [19], and 2.8 Å for $\rho = 3.175$ g/cm^3 and 2.85 Å for $\rho = 3.0$ g/cm^3 in our simulations. This last value is comparable to the value estimated by Waseda et al. for this peak, 2.8 Å, using a density of 3.01 g/cm^3. However, aside from this coincidence, which seems to be a systematic deviation of two different MD simulations, our findings are very different from the ones reported by Waseda et al.

Let us compare the structural results obtained for liquid alumina to some allotropic forms of Al$_2$O$_3$. As we noted in the Introduction, molten alumina is one of the precursors of metastable polymorphs; in particular, the following phase transformation towards the stable α-Al$_2$O$_3$ phase is known:

$$\text{melt} \rightarrow \gamma \rightarrow \delta, \quad \theta \rightarrow \alpha\text{-Al}_2\text{O}_3,$$
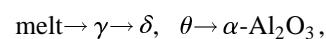
TABLE II. Density, coordination number, Al—O bond length, and ring statistics in terms of n-fold rings, for liquid alumina and the crystal phases γ-, θ-, and α-Al$_2$O$_3$. Name and mass density are given in the first and second columns, respectively. In the third column the coordination number of Al as well as of O atom are given, with its respective percentage in brackets. Bond length is given in the fourth column, the upper number is the Al—O distance with higher multiplicity, and the lower number is the range of the bond length. In the last column we present the percentage of n-fold rings, from two-fold to six-fold rings.

Phase	Density (g/cm^3)	Coordination number	Bond length Al-O (Å)	Ring distribution (%)				
				2	3	4	5	6
Liquid	3.175	Al: 3(13%), 4(66%), 5(20%)	1.75	13	24.6	31.6	22.6	7.5
		O: 2(31%), 3(61%), 4(6%)	(1.71-1.79)					
γ	3.66	Al: 4(30%), 6(70%)	1.941	40	40	18.5	1.5	0
		O: 3(50%), 4(44%), 5(6%)	(1.77–2.24)					
θ	3.6-3.65	Al: 4(50%), 6(50%)	1.904	23	62	15	0	0
		O: 3(66.6%), 4(33.3%)	(1.71–2.03)					
α	3.98	Al: 6(100 %)	1.97, 1.85	40	60	0	0	0
		O: 4(100 %)						

and in general, crystallization goes to phases containing both tetrahedrally and octahedrally coordinated aluminum. Table II shows some calculated structural properties of the liquid in order to compare to γ, θ, and α alumina polymorph [35,39,40]. Crystal phases are denser than the liquid, as well as present longer bond length and larger fraction of octahedrally coordinated Al atoms. This is consistent with the fact that the liquid has a lower coordination than the crystal phases, so its bond length will also be shorter. Moreover, the ring distribution shows that the fraction of four-fold, five-fold, and six-fold rings decreases as the density increases, and are not present at all in the octahedral α phase. A similar behavior have been observed in the case of SiO$_2$ [36]. According to the coordination numbers, it seems that the liquid state resembles more the θ than the γ phase. Therefore, it should be more probable to get the θ phase when liquid alumina is quenched from the melt. However, we think that this is not true, because here we only consider the bulk properties, and the surface structure of the γ phase has different structural properties. It has been suggested that the surface of γ-alumina could be considered as an amorphouslike phase [37]. In fact, the coordination numbers of the simulated surface agree with the ones of the liquid, and show an even better agreement with the coordination number of amorphous alumina [34].

In conclusion, we have performed MD simulations of liquid Al$_2$O$_3$, which support the recent experimental measurement presented by Ansell et al. [14] within the temperature range studied, and disagree with previous experimental results of Waseda et al. From our results we conclude that the structure mainly consist of a tetrahedral basic unit $(AlO_4)^{-5}$, linked through corners, edges, and faces. Moreover, we conclude that most of these tetrahedra are connected between them by an oxygen atom which links three tetrahedra to each other.

ACKNOWLEDGMENTS

[1] K. Wefers and C. Misra, Alcoa Tech. Pap. No. 19 (revised), 1997 (unpublished).

[2] I. Levin and D. Brandon, J. Am. Ceram. Soc. **81**, 1995 (1998).

[3] W. D. Kingary, *Introduction to Ceramics* (John Wiley, New York, 1960).

[4] P. Tyrolerova and W.K. Lu, J. Am. Ceram. Soc. **52**, 77 (1969).

[5] J.K.R. Weber, P.C. Nordine, and S. Krishnan, J. Am. Ceram. Soc. **64**, 3067 (1988).

[6] S. Krishnan, J.K.R. Weber, R.A. Shiffman, and P.C. Nordine, J. Am. Ceram. Soc. **74**, 881 (1991).

[7] J.P. Coutures, D. Massiot, C. Besseda, P. Echegut, J.C. Rifflet, and F. Taulelle, C. R. Acad. Sci., Ser. II: Mec., Phys., Chim., Sci. Terre Univers **310**, 1041 (1990).

[8] D. Massiot, F. Taulelle, and J.P. Coutures, Colloq. Phys. **C5**, 425 (1990).

[9] R.K. Sato, P.F. McMillan, P. Denison, and R. Dupree, J. Phys. Chem. **96**, 4483 (1991).

[10] B.T. Poe, P.F. McMillan, B. Cote, D. Massiot, and J.P. Coutures, J. Phys. Chem. **96**, 8220 (1992).

[11] J.K.R. Weber, C.D. Anderson, D.R. Merkley, and P.C. Nordine, J. Am. Ceram. Soc. **78**, 577 (1995).

[12] G. Shen and P. Lazor, J. Geophys. Res. **100**, 176 99 (1995).

[13] Y. Waseda, K. Sugiyama, and J.M. Toguri, Z. Naturforsch., A: Phys. Sci. **50**, 770 (1995).

[14] S. Ansell, S. Krishnan, J.K.R. Weber, J.J. Felten, P.C. Nordine, M.A. Beno, D.L. Price, and M.-L. Saboungi, Phys. Rev. Lett. **78**, 464 (1997).

[15] C.G. Levi, V. Jayaram, J.J. Valencia, and R. Mehrabian, J. Mater. Res. **3**, 969 (1988).

[16] M. Allen and D. Tildesley, *Computer Simulation of Liquids*

(Clarendon Press, Oxford, 1987).

[17] A.B. Belonoshko, Phys. Chem. Miner. **25**, 138 (1998).

[18] R. Ahuja, A.B. Belonoshko, and B. Johansson, Phys. Rev. E **57**, 1673 (1998).

[19] M.A. San Miguel, J. Fernández, L.J. Alvarez, and J.A. Odriozola, Phys. Rev. B **58**, 2369 (1998).

[20] K.T. Thomson, R.M. Wentzcovitch, and M.S.T. Bukowinski, Science **274**, 1880 (1996).

[21] W. Duan, R.M. Wentzcovitch, and K.T. Thomson, Phys. Rev. B **57**, 10 363 (1998).

[22] L.J. Alvarez, J. Fernández, M.J. Capitán, and J.A. Odriozola, Chem. Phys. Lett. **192**, 463 (1992).

[23] J.D. Gale, C.R. Catlow, and W.C. Mackrodt, Modell. Simul. Mater. Sci. Eng. **1**, 73 (1992).

[24] S. Blonski and S.H. Garofalini, Surf. Sci. **295**, 263 (1993).

[25] M. Matsui, Miner. Mag. **58A**, 571 (1994).

[26] F.H. Streitz and J.W. Mintmire, Langmuir **12**, 4605 (1996).

[27] M. Wilson, M. Exner, Y. Huang, and M.W. Finnis, Phys. Rev. B **54**, 15 683 (1996).

[28] C. Rambaut, H. Jobic, H. Jaffrezic, J. Kohanoff, and S. Fayeulle, J. Phys.: Condens. Matter **10**, 4221 (1998).

[29] M. Matsui, Phys. Chem. Miner. **23**, 345 (1996).

[30] M. Matsui, Geophys. Res. Lett. **23**, 395 (1996).

[31] K. Refson, MOLDY, Release 2.13, 1998, a general-purpose molecular dynamics code. Available free at http://www.earth.ox.ac.uk/~keith/moldy.html.

[32] J.R. Rustad, D.A. Yuen, and F.J. Spera, Phys. Rev. A **42**, 2081 (1990).

[33] As far as we know, there are three reported density for liquid alumina: 3.175 g/cm^3 [4], 2.97 g/cm^3 at $T = 2373$ K [38], and 3.01 g/cm^3 in E.E. Shpil'rain, K. A. Yakimovich, and A. F. Tsitsakin, High Temp.-High Pressure **5**, 191 (1973).

[34] G. Gutiérrez and B. Johansson (unpublished).

[35] We have calculated these numbers using the structural parameters given in Ref. [39] for α alumina, and in Ref. [40] for γ and θ alumina.

[36] W. Jin, R.K. Kalia, P. Vashishta, and J.P. Rino, Phys. Rev. B **50**, 118 (1994).

[37] L.J. Alvarez, L.E. León, J. Fernández, M.J. Capitán, and J.A. Odriozola, Phys. Rev. B **50**, 2561 (1994).

[38] M. Allibert *et al.*, *Slag Atlas*, edited by Verein Deutscher Eisenhüttenleute (Verlag Stahleisen, Düsseldorf, 1995), pp. 317 and 318.

[39] N. Ishizawa, T. Miyata, I. Minato, F. Marumo, and S.I. Iwai, Acta Crystallogr., Sect. B: Struct. Crystallogr. Cryst. Chem. **36**, 228 (1980).

[40] R.S. Zhou and R.L. Snyder, Acta Crystallogr., Sect. B: Struct. Sci. **47**, 617 (1991).